

## Dae Hoon Lee

Division of Aerospace Engineering,  
Korea Advanced Institute of Science and  
Technology,  
373-1 Kusung-dong, Yuseong-Gu,  
Taejon 305-701,  
Korea

## Dae-Eun Park

## Euisik Yoon

Division of Electrical Engineering,  
Korea Advanced Institute of Science and  
Technology,  
373-1 Kusung-dong, Yuseong-Gu,  
Taejon 305-701,  
Korea

## Sejin Kwon

e-mail: melody@kaist.ac.kr  
Department of Mechanical Engineering,  
Division of Aerospace Engineering,  
Korea Advanced Institute of Science and  
Technology,  
373-1 Kusung-dong, Yuseong-Gu,  
Taejon 305-701,  
Korea

# A MEMS Piston-Cylinder Device Actuated by Combustion

*Combustion measurement in a cylindrical micro combustor, the construction procedure and test run of a MEMS reciprocating device are described. The sizing of the MEMS device was based on the findings of combustion measurements. Thermodynamic analysis of the pressure measurement resulted in available work up to 2.4 Joules in a combustor height of 2 mm and more with combustion efficiency of 0.6~0.7. With combustor height less than 2 mm, combustion was incomplete due to excessive heat loss to the wall. In order to achieve the chamber height imposed by the combustion measurement, a fabrication process and wafer material that allow deeper etching was used.*

[DOI: 10.1115/1.1565095]

*Keywords:* Combustion, Combustors, Heat Transfer, Internal, Microscale, Reacting

## 1 Introduction

As the demand for power sources to actuate mobile micro systems increases, micro scale heat engines have been tested as an alternative to batteries. Particularly when micro systems are required to perform mechanical work as in a micro air vehicle and micro spacecraft, the drain of energy is too quick for batteries to be a viable energy source. Although the power requirement of micro system is substantially less than macro scale devices, mobile micro systems have stringent weight and packaging limitations for power sources. In general, the energy density of batteries is too low for use where mechanical power is needed. On the other hand, the smallest existing engines in model aircraft are still too bulky and unreliable for applications in micro systems. The energy density of hydrocarbon liquid fuel is approximately 1000 times that of batteries. Even if we take into account the low thermal efficiency caused by reducing the scale of the device, power generation using a micro combustor may be an attractive alternative.

In recent years, several research groups started working on concepts of micro scale combustion devices. Fu et al. [1] described work on a MEMS rotary engine and Mehra et al. [2] tested a prototype MEMS turbine engine that was fabricated by wafer bonding and Deep RIE. Sitzki et al. [3] reported an experiment on a micro scale excess enthalpy burner. While the fabrication processes of MEMS devices have matured, combustion phenomena at micro scale have not yet been explored, partly because need for research has arisen recently.

We expect that a variety of constraints in a millimeter or sub-millimeter scale combustion chamber have been ignored in a macro scale heat engine, when combustion occurs. Firstly, the

sizing of a combustor is dictated by combustion in a micro scale environment. As noted above, literature is scarce in this area. Except the quenching distance measured between two discs, data on the lower limit of a combustor scale that allows burning are not adequate for design and evaluation of such devices. As the combustor size is reduced to a scale comparable to or less than quenching distance, processes that have been ignored in a macro scale combustion become significant. Increased heat transfer through the combustor wall affects both the flame propagation and the cooling of burnt gases after burning is completed. Secondly, the small-scale combustor volume has adverse effects on the ignition of the fuel and air mixture. For stable initiation of combustion, a relatively large heat input is required in terms of electric discharge or catalytic reaction in some cases. When electric spark discharge is used for ignition, electrical insulation must be provided between the electrodes and the combustor walls without increasing the overall volume of the device, common silicon wafer material is not a good insulator and not suitable as a base plate material in an electrically ignited combustor as a result. Work on ignition by micro scale electric discharge, thermal heating and catalytic reaction have been reported by different research groups [4–6]. Thirdly, a practical micro engine requires a number of micro fluidic devices to meter and calibrate fuel and oxidizer flows. Due to the progress in MEMS devices in the past decades, there is a wide variety of available technology in micro fluidic devices including valves and pumps [7]. Lastly, we need an estimate of available work from combustion in a micro combustor. The theoretically available work in terms of the second law of thermodynamics must be sufficiently high for the combustor to produce work.

In order to solve all the technical problems in the development of a micro engine, a systematic investigation involving many different disciplines is necessary. Two of the most pressing tasks in the design of a micro engine are the understanding the combustion process in a micro scale volume and developing fabrication pro-

Contributed by the Heat Transfer Division for publication in the JOURNAL OF HEAT TRANSFER. Manuscript received by the Heat Transfer Division April 12, 2002; revision received December 26, 2002. Associate Editor: R. Skocypec.

cesses to materialize such a device. Past research on micro combustion devices placed emphasis on the fabrication processes and performance verification of subsystems and overlooked the importance of the thermo-fluidic phenomena of micro combustion. In the present study, combustion phenomena in a micro cylinder with variable depth were investigated experimentally and simple model was derived to predict the quenching. The results of the combustion study were applied to the design of a micro-reciprocating device powered by combustion for sizing and performance estimation. A micro machining process was established to accommodate the scale requirement imposed by the combustion experiment and modeling. Finally, a prototype device was constructed and a single stroke operation was tested successfully.

## 2 Design and Feasibility

**2.1 Combustion Experiment.** A miniature closed vessel combustion chamber with a cylindrical inside volume was designed and fabricated with a variable depth from 0.4 to 4 mm [8]. A stoichiometric mixture of hydrogen and air was supplied to the combustor. A piezoelectric pressure transducer inserted through the chamber wall picked up the instantaneous pressure hike after ignition and the subsequent pressure drop after completion of reaction.

The ratio of the peak pressure to the initial pressure is plotted in Fig. 1 for the cases tested. Eight realizations of each test condition were made to obtain statistically significant results. The scatter of individual measurement ranged from 3 to 17% around the mean values and has an average of 7% with a significance, tested by significance level of 5%. The deviations are represented by error bars on the plot. This ratio represents a measure of the mean effective pressure of the burnt gases and has significance in evaluating the available work. Also, the value is used for the determination of the heat transfer coefficient for thermal analysis. The plot shows that the pressure ratio is nearly independent of the initial pressure for a combustion chamber height less than 2.0 mm. With bigger combustion chamber volumes, the pressure ratio responded favorably to higher initial pressure.

The effect of heat loss to the surroundings is related to the shape parameter, which is defined as the ratio of surface to volume of the cylinder. Figure 2 shows the effect of the shape parameter on the pressure ratios that is averaged over each initial pressure ratio in Fig. 1. The error bars on this plot represent the extent of deviation of the ratio of peak pressure to initial pressure. The deviation decreases and the pressure ratio becomes independent of

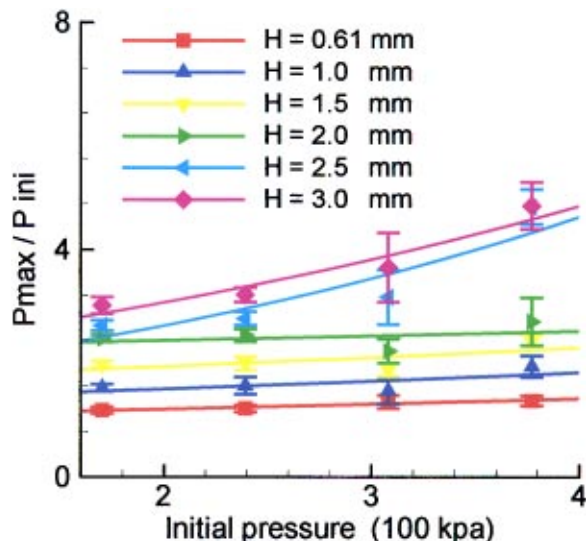


Fig. 1 Maximum to initial pressure ratio in each test condition

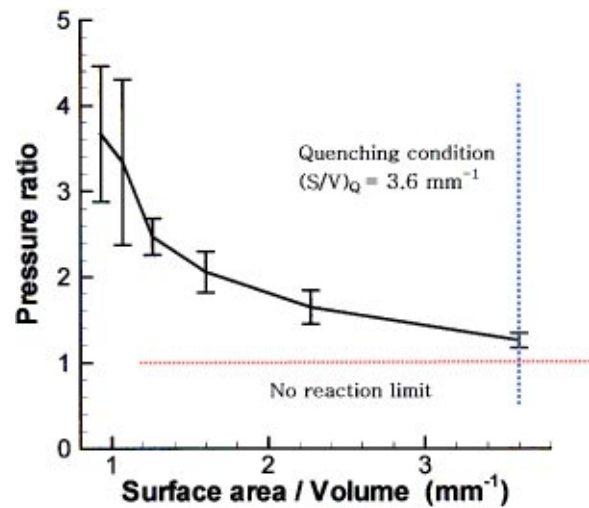


Fig. 2 Pressure ratio plotted against shape factor

initial pressure as the combustor size decreases. The vertical dotted line, toward the higher value of shape parameter, is the surface to volume ratio evaluated from existing data of quenching distance [9]. The horizontal dotted line represents a pressure ratio of unity, implying no combustion. The measured pressure ratio starts high at low shape parameter and decreases toward unity as the shape parameter increases. This figure qualitatively demonstrates combustion efficiency is significantly lower in a micro scale combustion chamber than in a macro scale. However, pressure data alone are inadequate for the quantitative estimation of the combustion efficiency.

**2.2 Quenching Prediction.** The present calculation employs a simple theoretical model rather than a direct numerical simulation to predict quenching and combustion efficiency. It is based on energy balance equation within closed vessel combustor [10]. In the modeled MEMS combustor, the flame is assumed to propagate in a shallow cylindrical volume with a depth of a few millimeters at most. The flame propagates in a radial direction while the dominant heat transfer is towards the top and bottom walls. Unlike combustion in a macro scale volume, the heat loss actively affects the flame propagation and must be accounted for in the integration of the equation that governs the flame motion.

The flame propagation is divided into many small consecutive steps. Upon completion of each propagation step, the system is adjusted by the heat loss during the step. Assumptions made for the modeling follow Lee and Kwon [11]. Figure 3 shows the

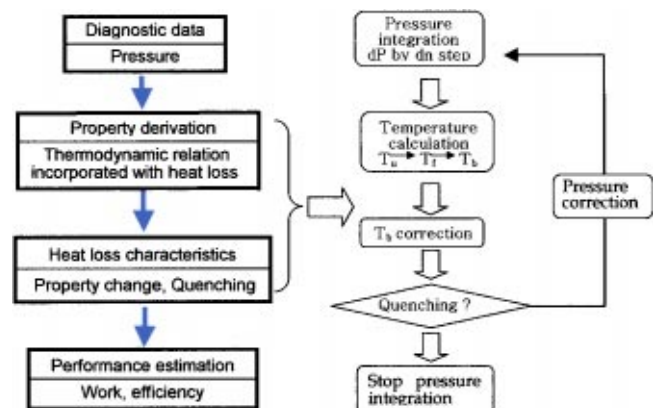


Fig. 3 Schematic diagram for solution procedure

calculation procedure of the model. For each small step of flame propagation, the pressure and temperature are corrected by the adiabatic compression and the heat loss to the wall. The step size of the flame propagation was about the scale of the flame thickness to ensure the convergence of calculation. For each step, the heat generated by the combustion is compared to the heat loss to the wall to test the quenching condition. The total heat loss is the sum of wall heat transfer and conduction to the unburned region and is expressed as  $(2n/H)Vh(T_b - T_\infty) + A_f k \Delta T_f / \delta_f$ . If heat production from the advancement of the flame is less than the total loss, quenching has occurred. The simplified equations to be solved simultaneously are as follow [10].

Pressure-burned fraction relation

$$\frac{dP}{dn} = \frac{(\beta(P/P_i)^{1/\gamma_u} - 1) \cdot P}{1/\gamma_b \cdot (P/P_i)^{1/\gamma_u} - (1/\gamma_b - 1/\gamma_u)(1-n)} \quad (1)$$

Pressure-temperature relation

$$T_u = T_i \left( \frac{P_u}{P_i} \right)^{1-1/\gamma_u} \quad (2)$$

$$m_e c_{p(b)} T_f = [m_i c_{p(u)} \cdot T_u + m_i \cdot \chi_{H_2} \dot{h}_{H_2}] \quad (3)$$

$$T_{bj} = T_{fk} \left( \frac{P_k}{P_j} \right)^{1-1/\gamma_b} \quad (4)$$

Where,  $j$  is an index for an arbitrary spatial location in the burnt region, while  $k$  is an index of the flame location.

Equation (1)–(4) are normalized by initial temperature and pressure in the following Eqs. (5)–(8). The cooling step and quenching condition, also expressed in normalized form, are presented in Eqs. (9)–(10)

$$\frac{d\pi}{dn} = \frac{(\beta\pi^{1/\gamma_u} - 1) \cdot \pi}{1/\gamma_b \cdot \pi^{1/\gamma_u} - (1/\gamma_b - 1/\gamma_u)(1-n)} \quad (5)$$

$$\theta_u = \pi^{1-1/\gamma_u} \quad (6)$$

$$\theta_f = \left[ \frac{m_i c_{p(u)}}{m_e c_{p(b)}} \cdot \theta_u + \frac{m_i}{m_e c_{p(b)} T_i} \cdot \chi_{H_2} \dot{h}_{H_2} \right] \quad (7)$$

$$\theta_b = \theta_f \cdot \left( \frac{\pi}{\pi_f} \right)^{1-1/\gamma_b} \quad (8)$$

$$[\theta_b - \theta_f] = \frac{2nh}{m_e c_{p(b)} H} (\theta_b - \theta_\infty) + \frac{A_f k}{V n m_e c_{p(b)} \delta_f} (\theta_f - \theta_u) \quad (9)$$

$$\delta_L m_i \chi_{H_2} \dot{h}_{H_2} \leq \frac{2nVhT_i}{H} (\theta_b - \theta_\infty) + \frac{A_f k T_i}{\delta_f} (\theta_f - \theta_u) \quad (10)$$

Equation (1) is the relationship between pressure and burned volume fraction inside the cylinder. Equation (2) to (4) are relationships between gas properties assuming ideal gas and instantaneous isentropic compression due to flame propagation substeps. Equation (4) is the expression of frozen isentropic relation between any location in burned region and flame [12]. Equation (9) represents the conservation of energy including the heat loss to the combustor wall as well as to the unburned region. Equation (10) is the quenching condition that will be tested upon completion of each flame propagation step. Equation (5)–(9) constitute a system of equations and solved simultaneously for  $\pi$ ,  $\theta_f$ ,  $\theta_u$ ,  $\theta_n$ ,  $n$  with a known heat transfer coefficient.

Figure 4(a) shows the pressure-burnt fraction relationship obtained by integrating Eq. (5) and Fig. 4(b) is the ratio of the heat loss (the right hand side of Eq. (10)) to the heat of combustion (the left hand side of Eq. (10)) as a function of burnt fraction for various values of  $h$ . Flame is quenched when this ratio reaches unity and pressure attains its peak at that burnt fraction. The procedure for determination of the heat transfer coefficient from the measured peak pressure is as follows: (1) guess  $h$ , (2) find burnt fraction at quenching from Fig. 4(b), (3) find peak pressure from

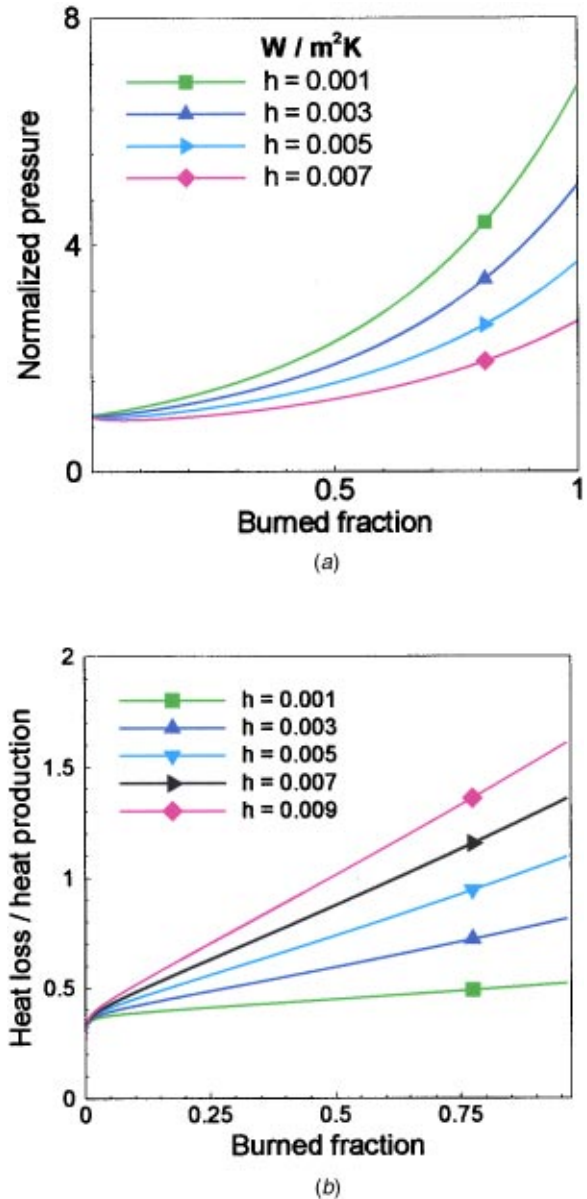


Fig. 4 Heat loss effect on pressure buildup and heat loss to heat production ratio: (a) pressure change for the assigned  $h$  value; and (b) the ratio of heat loss to production for the assigned  $h$  value.

Fig. 4(a) with the same  $h$  and burnt fraction, and (4) if the resulting peak pressure is largely different from the measured peak pressure, correct  $h$  and repeat (2) and (3) until the discrepancy between the calculated and measured peak pressures fall within a tolerance limit. The procedure is illustrated in Fig. 5.

The numerical integration was performed by the second order Runge-Kutta method which has a numerical uncertainty of the order of  $(dn)^3$ , where  $dn$  is the integration step size. We used 0.01 for  $dn$ , which resulted in the computational uncertainty with an order of  $10^{-6}$ .

Figure 6 shows the temperature profiles as a function of burnt fraction at two typical instances during the flame propagation. In Fig. 7, the heat transfer coefficients determined at different test conditions are presented as a function of the initial pressure with the cylinder depth as a parameter. Figure 7 shows the dependence of heat transfer coefficient on the combustor height and initial pressure.

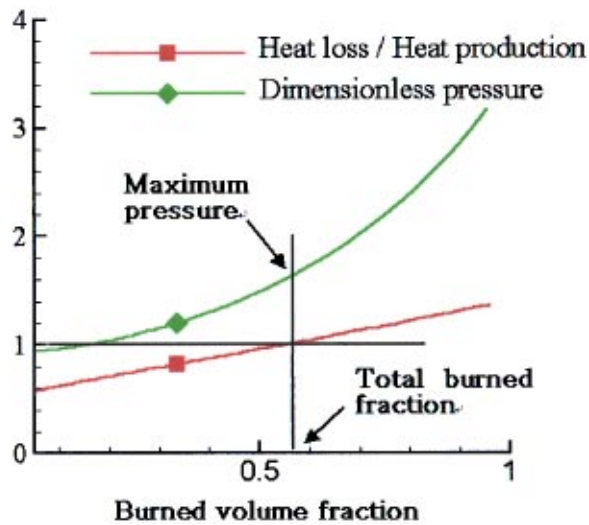


Fig. 5 Determination of total burned fraction in experiment case

**2.3 Second Law Analysis.** Total burned fractions that were obtained from the quenching calculation at all test cases are presented in Fig. 8. From the result of total burned fraction quenching is observed in most cases. The result can be used to calculate heat produced by the combustion process which experiences quenching. Also it can be used as design parameter as upper limit of device dimension to prevent quenching in combustor. The work available from a hot gas system is estimated from the gas properties in a closed system undergoing a quasi-equilibrium process from the peak pressure to quenching [13] by

$$m_{\text{Total}} = m_e + m_u$$

$$W_{\text{rev}} = (m_{eb}u_e - m_{ib}u_i) + (m_{iu}u_e - m_{iu}u_i) - T_{\infty} \{ (m_{eb}s_e - m_{ib}s_i) + (m_{iu}s_e - m_{iu}s_i) \} \quad (11)$$

Where, subscript *i* denotes the initial state and subscript *e* the state at the instant the flame stops. The available work is plotted in Fig. 9. With chamber depth greater than 2 mm, the hot gas generated by combustion can theoretically produce 0.5 to 2.4 J per

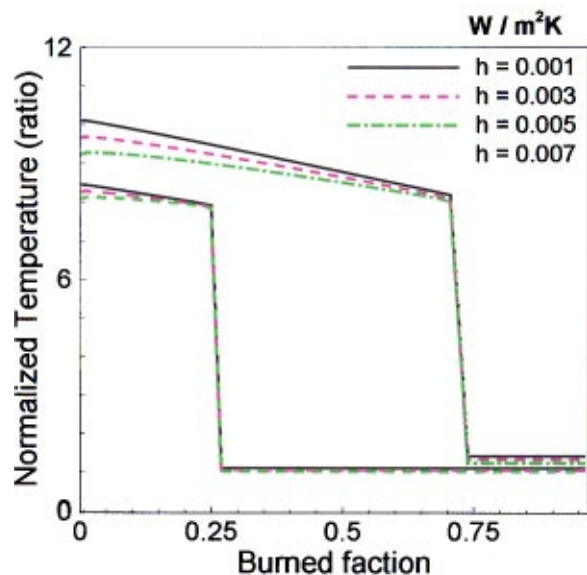


Fig. 6 Heat loss effect on temperature propagation

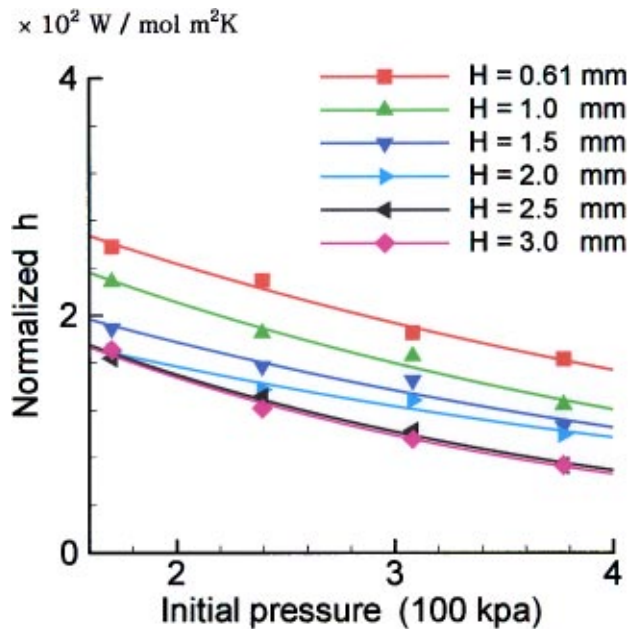


Fig. 7 Heat transfer coefficient normalized by initial molar mass

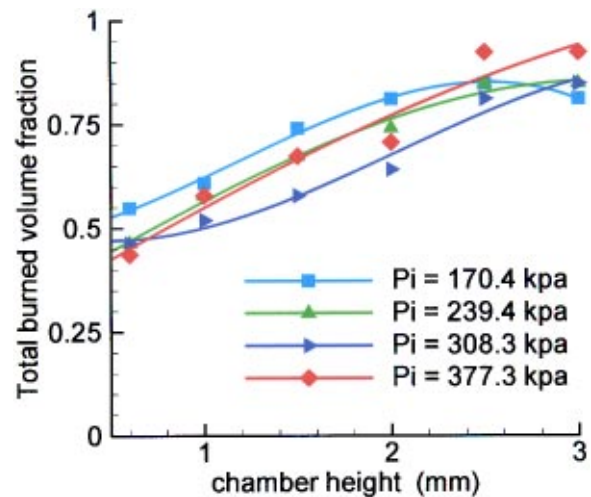


Fig. 8 Total burned fraction of all test cases

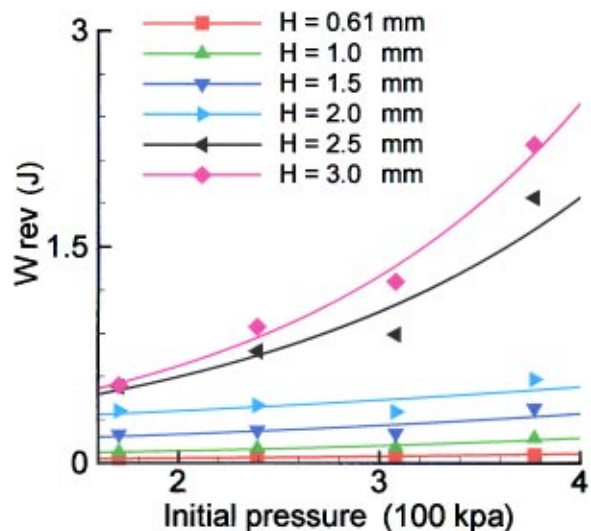


Fig. 9 Estimated reversible work

cycles. From comparison of the estimated reversible work, the combustion efficiency is evaluated. Combustion efficiency is defined by

$$\eta = \frac{W_{rev}}{\dot{n}_{H_2} m_i \chi_{H_2}} \quad (12)$$

For all experimental conditions, the combustion efficiency was between 0.6 and 0.7, which is lower than macro scale combustors as expected.

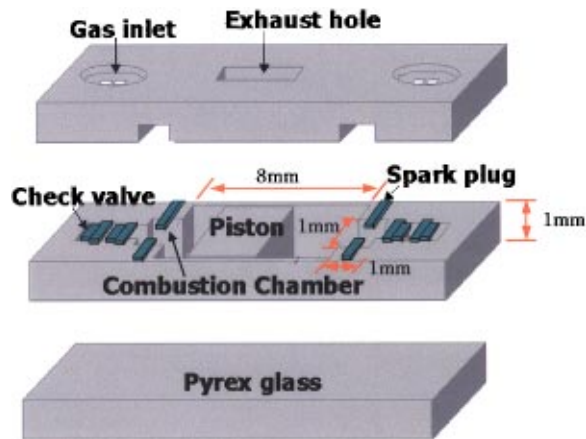


Fig. 10 Proposed structure of MEMS engine

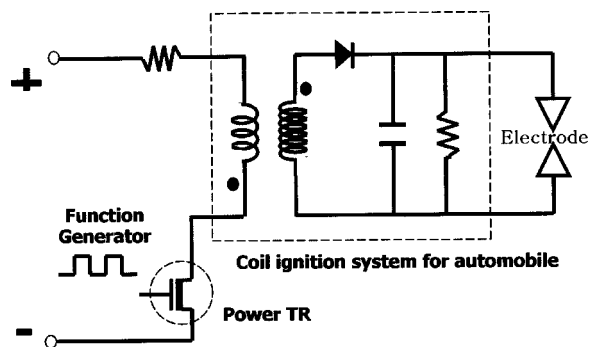


Fig. 11 Schematic of coil ignition system

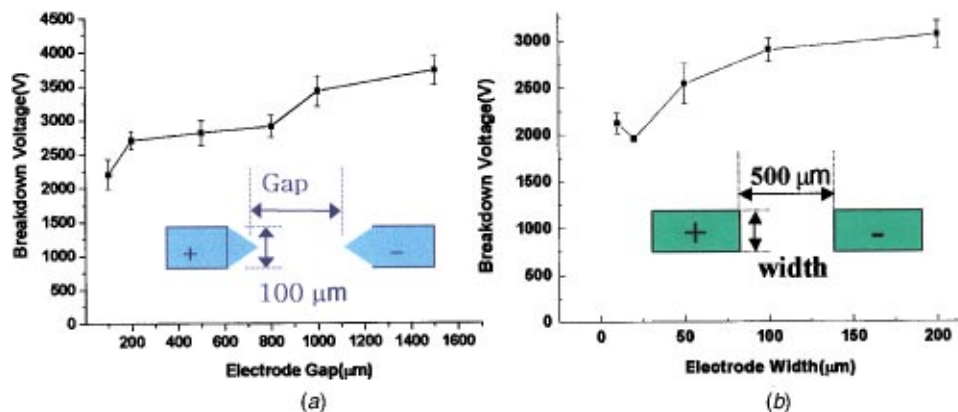


Fig. 12 Discharge voltage according to electrode gap: (a) gap versus discharge voltage; and (b) width versus discharge voltage

### 3 Micro Fabrication of the Device

**3.1 Proposed Design.** The experimental data were used in the design of a micro reciprocating device. In this part, the design, fabrication process and actual combustion test of a prototype reciprocating device are described. The design concept tested here can be further developed and incorporated into a micro engine system. The engine structure consists of three wafer layers bonded together. Photosensitive glass was selected as base material for two reasons: glass wafer itself is a good electrical insulator than Si wafer and anisotropic etching produces better result with a photo-sensitive glass. The middle layer is also made of photosensitive glass wafer and the cylinder and the combustion chamber are engraved on this layer. The bottom layer is made of Pyrex glass wafer and serves as a base plate of the assembly. The schematic of the device is illustrated Fig. 10. The initial combustor volume was  $1\text{ mm} \times 1\text{ mm} \times 1\text{ mm}$  with a stroke length of 8 mm. The design is a result of compromise between competing requirements of the fabrication and the combustion. The smaller the chamber height, the easier and cheaper the fabrication process becomes, because the device can be built on an off-the-shelf wafer that are usually available in thickness of 1 mm.

**3.2 Ignition.** Ignition is required to initiate combustion in the device. In the present study, an electric spark was used to accurately calibrate the ignition energy. The ignitor circuitry is integrated onto the wafer on which the device is built during the micro machining process of the overall device. The construction of the ignitor should take into account the minimum ignition energy for the given gas mixture and integration with the overall device. We used Ni electroplating to build the ignition circuitry and electrodes on the wafer material [14]. The electroplated Ni layer on the base plate was  $40\ \mu\text{m}$  high and  $20\sim 200\ \mu\text{m}$  wide. A schematic of an inductance type ignition system used in the experiment is shown in Fig. 11. The ignition energy of  $1.7\sim 1.8\text{ mJ}$  was sufficient to ignite the combustible gas and much smaller than the available work.

Effects of electrode geometry on the discharge voltage are shown in Fig. 12. The endurance of the electrodes was tested by discharging an electric spark at a frequency of 1 kHz. The test result in Fig. 13 shows growth of erosion at the tip of the electrodes. However, the spark discharge did not show further deterioration up to  $10^6$  operations.

**3.3 Fabrication Process.** The fabrication process for each layer is described below, beginning with the middle layer. Photosensitive glass of thickness 1 mm is exposed to UV light and thermally treated. UV intensity was controlled to  $8\text{ J/cm}^2$  at a wavelength of 350 nm. The wafer was then etched slightly to make a depth coverage that could be used as an align key. A

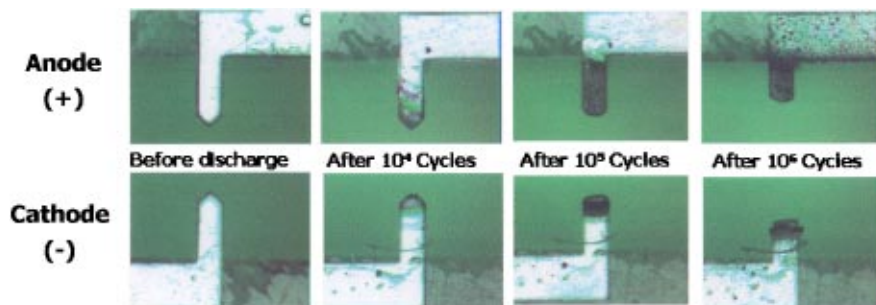


Fig. 13 Result of reliability test of fabricated electrode

Cr/Au seed layer was deposited for the electroplating process with a thermal evaporator with a thickness of  $250 \text{ \AA}/2500 \text{ \AA}$ . A thick PR (AZ9260) mold was formed on top of the wafer with a thickness of  $45 \text{ \mu m}$ . A  $40 \text{ \mu m}$  deep Ni layer was electroplated on top of it. The UV-exposed and thermally treated glass was etched in an HF solution with 10% of HF concentration by volume. The use of an ultrasound washing device accelerated the etching to  $20 \text{ \mu m}/\text{min}$ . The glass wafer was etched from the backside to protect the seed layer and Ni structure during the etching process. For additional protection, the front side was coated with a paraffin layer. After completion of etching, paraffin and AZ 9260 PR are stripped by boiling in TCE(Trichloroethylene), acetone, and methanol solutions, in that order.

The same process is used for the top layer with a reduced UV intensity of  $3 \text{ J}/\text{cm}^2$ , as the etching depth for the top layer is approximately half the thickness of the wafer. This is because the upper and lower halves are patterned differently.

The bottom and middle layers were bonded together and a piston made of photosensitive glass was inserted into the cylinder. Lastly, the top layer was bonded to the middle layer with epoxy glue. Since the piston must remain free, fusion bonding of the middle layer and the top layer is not suitable in this structure. This process is not complex but causes the problem of gas leakage through a gap resulting from the epoxy bonding. Although not used in the present study, fusion bonding is expected to result in better seal against gas leakage. Aside from the unsealed gap of tens of microns caused by bonding of the different layers, there is also a gap between the side face of the piston and the cylinder

wall. Gas leakage through these gaps undermines the performance of a heat device. For better construction, better bonding methods with possible lubricant on the sidewall of the cylinder can be considered.

**3.4 Results.** The final fabricated device is shown in Fig. 14. A combustion test was carried out with the prototype device. Test was performed with stoichiometric mixture of hydrogen and air at atmospheric pressure. The results suggest proper ignition and flame propagation within the cylinder. Analyzing the piston displacements of consecutive video images, piston velocity was derived. Image analysis of the video clip taken at a framing rate of 9000 fps by a digital motion analyzer resulted in the piston speed of approximately  $10 \text{ cm}/\text{stion gas}$ . Relatively low piston speed is partly anticipated due to incomplete sealing of the cylinder. For the temperature measurement, monolithically implanted micro-resistance appears promising but was not tried in the present study.

## 4 Conclusion

A MEMS combustion device was built and its operation was demonstrated. The design was based on data obtained from a combustion experiments in a micro combustor. Simple pressure measurement and visualization of the test combustor resulted in data for sizing and prediction of performance of the device. When the combustion chamber had a height less than  $2 \text{ mm}$ , quenching and increased heat loss prevented stable ignition and completion of combustion. Partial flame propagation and subsequent pressure rise was observed even in a combustor depth slightly less than the quenching distance. Theoretical analysis based on the measured pressure data resulted in thermal energy release up to a few Joules in a combustor height of  $2 \text{ mm}$  and more. Combustion efficiency was about  $0.6\sim 0.7$ , which is lower than in a macro scale combustor. In order to achieve higher efficiency, additional measures such as preheating and/or insulation of the wall may prove effective.

Based on the findings of the micro combustion experiment and the theoretical analysis, a MEMS reciprocating device was designed and a fabrication process was established. Photosensitive glass was proven to be suitable for the reciprocating combustion device for its favorable material properties, namely, high electric resistance, anisotropic etching characteristics and low thermal conductivity.

A combustion test of the reciprocating device showed piston displacement by hot gases. Although plagued with the leakage problem aforementioned, the test demonstrated that a micro-scale reciprocating device can be built and power can be generated. The findings of the present study warrant further research on micro combustion phenomena and different concepts of micro engines.



Fig. 14 Fabricated result

## Nomenclature

$A$  = area  
 $C_p$  = specific heat  
 $H$  = combustor height  
 $h$  = heat loss coefficient  
 $\dot{h}$  = heating value  
 $k$  = thermal conductivity  
 $m$  = mole number  
 $n$  = burned fraction  
 $P$  = pressure  
 $s$  = entropy  
 $T$  = temperature  
 $u$  = internal energy  
 $V$  = combustor volume  
 $W$  = work

## Subscripts

$b$  = burned  
 $e$  = after completion of combustion  
 $f$  = flame surface, at flame  
 $i$  = initial  
 $L$  = laminar  
 $u$  = unburned  
 $\infty$  = surrounding

## Greek

$\beta$  = ratio of burned region temperature after and before compression  
 $\chi$  = mole fraction  
 $\delta$  = thickness  
 $\gamma$  = specific heat ratio  
 $\eta$  = combustion efficiency  
 $\pi$  = non dimensional pressure  
 $\theta$  = nondimensional temperature

## References

- [1] Fu, K., Knobloch, A. J., Cooley, B. A., Walter, D. C., Fernandez-Pello, C., Liepmann, D., and Miyasaka, K., 2001, "Microscale Combustion Research for Application to MEMS Rotary IC Engine," *Proc. ASME 35th National Heat Transfer Conference*, NHTC2001-20089.
- [2] Mehra, A., Ayon, A. A., Waitz, I. A., and Schmidt, M. A., 1999, "Microfabrication of High-Temperature Silicon Devices Using Wafer Bonding and Deep Reactive Ion Etching," *J. Microelectromech. Syst.*, **9**(2), pp. 152–160.
- [3] Sitzki, L., Borer, K., Schuster, E., Maruta K., Ronney, P. D., and Wussow, S., 2001, "Combustion in Microscale Heat-Recirculating Burners," *Proc. 3rd Asia-Pacific Conference on Combustion*, pp. 473–476.
- [4] Ono, T., Sim, D. Y., and Esashi, M., 2000, "Imaging of Micro-Discharge in a Micro-Gap Electrostatic Actuator," *Proc. 13th IEEE International Micro Electro Mechanical Systems Conference, MEMS'00*, pp. 651–654.
- [5] Kercher, D. S., Seriburi, P., and Allen, M. G., 1999, "An Experimental Study of Microfabricated Nickel Spark Plugs," *Proc. Solid State Sensors and Actuators Transducers '99*, pp. 1412–1415.
- [6] Srinivasan, R., Firebaugh, S. L., Hsing, I-M., Ryley, J., Harold, M. P., Jensen, K. F., and Schmidt, M. A., 1997, "Chemical Performance and High Temperature Characterization of Micromachined Chemical Reactors," *Proc. Solid State Sensors and Actuators, Transducers '97*, pp. 163–166.
- [7] Kovacs, G. T. A., 1998, *Micromachined Transducers-Sourcebook*, McGraw-Hill.
- [8] Lee, D. H., Choi, K. H., and Kwon, S., 2001, "Measurement and Modeling of Combustion in a Microcombustor," *Proc. AIAA 36th Thermophysics Conference*, AIAA 2001–3077.
- [9] S. R., Turns, 1996, *An Introduction to Combustion*, McGraw Hill, Singapore.
- [10] Lewis, B., and von Elbe, G., Combustion, *Flames and Explosions of Gases*, Academic Press, London, Chap. V. 15.
- [11] Lee, D. H., and Kwon, S., 2002, "Heat Transfer and Quenching Analysis of Combustion in a Micro Combustion Vessel," *J. Micromech. Microeng.*, **12**(5), pp. 670–677.
- [12] Takeno, T., and Iijima, T., 1985, "A Theoretical Analysis of Flame Propagation in Closed Vessel," *Trans. Japan Soc. Aero. Space Sci.*, **28**(79), pp. 1–15.
- [13] Cengel, Y. A., and Boles, M. A., 1989, *Thermodynamics—An Engineering Approach* 2nd ed., McGraw-Hill, p. 335.
- [14] Kercher, D. S., Seriburi, P., and Allen, M. G., 1999, "An Experimental Study of Microfabricated Nickel Spark Plugs," *Transducers '99 Sendai, Japan*, pp. 1412–1415.